A virtual control coupling approach for problems with non-coincident discrete interfaces

Pavel Bochev, Paul Kuberry, and Kara Peterson

Center for Computational Research,
Sandia National Laboratories*,
Albuquerque, NM 87125, USA,
{pbboche,pakuber,kjpeter}@sandia.gov,

Abstract. Independent meshing of subdomains separated by an interface can lead to spatially non-coincident discrete interfaces. We present an optimization-based coupling method for such problems, which does not require a common mesh refinement of the interface, has optimal H^1 convergence rates, and passes a patch test. The method minimizes the mismatch of the state and normal stress extensions on discrete interfaces subject to the subdomain equations, while interface "fluxes" provide virtual Neumann controls.

Keywords: PDE constrained optimization, mesh tying, transmission, non-coincident interfaces, optimal control, virtual Neumann controls.

1 Introduction

Solution of elliptic problems on two or more non-overlapping subdomains, subject to coupling conditions, occurs in multiple contexts. Independent meshing of these subdomains induces independent mesh partitions of the interface. In the more benign case the interface grids are non-matching but spatially coincident. However, when the interface is curved the induced interface grids may be spatially non-coincident, leading to gaps and/or overlaps between them. This complicates the accurate numerical solution of the coupled problem [1, 2]. We present a new, optimization-based formulation, which avoids some difficulties associated with the application of domain decomposition methods [3, 4] to such problems. Following [5, 6], we switch the roles of the coupling conditions and the subdomain equations by couching the interface problem into a virtual control formulation in which the former define the objective, the latter define the constraints, and the interface flux serves as a Neumann control. Section 2 summarizes the germane notation and states the model interface problem. The optimization-based formulation, including the necessary state and flux extension operators are presented in Section 3, while Section 4 contains several representative numerical examples. Section 5 summarizes our findings.

* Sandia National Laboratories is a multimission laboratory managed and operated by National Technology and Engineering Solutions of Sandia, LLC., a wholly owned subsidiary of Honeywell International, Inc., for the U.S. Department of Energy's National Nuclear Security Administration under contract DE-NA-0003525.

2 Notation and statement of the problem

Consider a bounded open region $\Omega \subset \mathbf{R}^d$, $d = 2, 3$ with a Lipschitz continuous boundary Γ. An interface σ splits Ω into two non-overlapping subdomains Ω_1 and Ω_2 with Dirichlet boundaries $\Gamma_i = \partial\Omega_i \backslash \sigma$, $i = 1, 2$. We assume that each subdomain is endowed with an independently defined conforming finite element mesh Ω_i^h, $i = 1, 2$ with elements $\boldsymbol{k}_i^n$. These meshes induce finite element partitions σ_1^h and σ_2^h of the interface σ, containing the element sides $\boldsymbol{s}_i^n$ that have all their vertices in σ. The geometrical entities described by σ_1^h and σ_2^h are two different "versions" of the interface, denoted by σ_1 and σ_2, respectively. These entities and their associated finite element partitions are not required to match or to be spatially coincident; see Fig. 1. Given a mesh entity μ we denote the sets of all mesh vertices in μ by $V(\mu)$. For example $V(\sigma_i^h)$ are the vertices in the interface mesh σ_i^h and $V(\Omega_i^h)$ is the set of all vertices in the subdomain mesh Ω_i^h. If μ is a finite set, then $|\mu|$ is its dimension, e.g., $|\sigma_i^h|$ is the number of elements in σ_i^h. If μ is a geometric entity, then $|\mu|$ is its measure, e.g., $|\boldsymbol{k}_i^n|$ is the volume (or area) of an element $\boldsymbol{k}_i^n$.

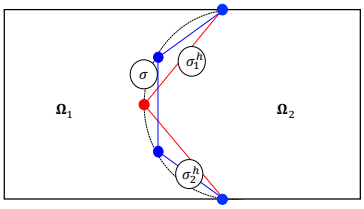

Fig. 1. Independent meshing of two subdomains separated by a curved interface σ results in two spatially non-coincident interface grids σ_1^h and σ_2^h.

We denote the standard Sobolev space of order one on Ω_i, $i = 1, 2$, and its subspace of functions with vanishing trace on Γ_i by $H^1(\Omega_i)$ and $H^1_{\Gamma_i}(\Omega_i)$, respectively. H_i^h is a conforming finite element subspace of $H^1(\Omega_i^h)$ with Lagrangian basis $\{N_i^k\}$, $H_{i,\Gamma}^h$ is a conforming subspace of $H^1_{\Gamma_i}(\Omega_i^h)$, $H_{i,\sigma}^h$ is the span of all basis functions associated with vertices on σ_i^h, and $T_i^h = H_{i,\sigma}^h\big|_{\sigma_i}$. The coefficient vector of $u_i^h \in H_i^h$ is $\boldsymbol{u}_i \in \mathbf{R}^{n_i}$, where $n_i = |H_i^h|$, the dimension of H_i^h.

In this paper we consider the model transmission problem

$$\begin{cases} -\nabla \cdot (\kappa_i \nabla u_i) = f_i \text{ in } \Omega_i, \;\; \text{i=1,2} & u_1 = u_2 \quad \text{on } \sigma \\ u_i = 0 \;\; \text{on } \Gamma_i, \;\; \text{i=1,2} & \kappa_1 \nabla u_1 \cdot \mathbf{n} = \kappa_2 \nabla u_2 \cdot \mathbf{n} \text{ on } \sigma \end{cases} \tag{1}$$

where $\mathbf{n}$ is unit normal on σ and, for simplicity, κ_i is a positive constant on Ω_i. In this paper we develop stable and accurate methods for (1) that can handle spatially non-coincident interfaces $\sigma_1 \neq \sigma_2$. Our approach is based on the reformulation of (1) into a PDE-constrained optimization problem with virtual Neumann controls. We start by splitting (1) into a pair of subdomain equations with mixed Dirichlet and Neumann boundary conditions, and weak forms given by *seek* $u_i \in H^1_{\Gamma_i}(\Omega_i)$ *such that*

$$\kappa_i(\nabla u_i, \nabla v_i)_{\Omega_i} = (f_i, v_i)_{\Omega_i} + \langle g_i, v_i \rangle_\sigma \quad \forall v_i \in H^1_{\Gamma_i}(\Omega_i), \; i = 1, 2. \tag{2}$$

We treat the Neumann data g_i as a virtual control and introduce the objective

$$\begin{aligned} J_\delta(u_1, u_2, g_1, g_2) = \frac{1}{2}\int_\sigma (u_1 - u_2)^2 dS + \frac{1}{2}\int_\sigma ((\kappa_1 \nabla u_1 - \kappa_2 \nabla u_2) \cdot \mathbf{n})^2 dS \\ + \frac{\rho}{2}\left(\int_\sigma g_1 dS + \int_\sigma g_2 dS\right)^2 + \frac{\delta_1}{2}\int_\sigma g_1^2 dS + \frac{\delta_2}{2}\int_\sigma g_2^2 dS \end{aligned} \tag{3}$$

The reformulation of (4) is then given by the following optimization problem

$$\text{minimize } J_\delta(u_1,u_2,g_1,g_2) \text{ over } H^1_{\Gamma_1}(\Omega_1)\times H^1_{\Gamma_2}(\Omega_2)\times L^2(\sigma) \text{ subject to (2).} \quad (4)$$

This problem provides the basis for our new method.

3 Virtual control formulation

For simplicity we consider C^0 piecewise linear elements on affine grids. When $\sigma_1 \neq \sigma_2$ we cannot discretize (4) directly because the interface integrals in (3) and (2) are undefined. We resolve this issue by using extension operators

$$E_{i,\gamma} : T_i^h \mapsto L^2(\sigma_\gamma) \text{ and } G_{i,\gamma} : \nabla T_i^h \mapsto [L^2(\sigma_\gamma)]^d, \quad \gamma \in \{1,2\}, \gamma \neq i. \quad (5)$$

to compare finite element fields defined on σ_i^h and their gradients to fields and gradients defined on σ_γ. The only requirement for these operators is consistency for linear and constant fields, respectively, i.e., $E_{i,\gamma}(p(\boldsymbol{x})) = p(\boldsymbol{x})\big|_{\sigma_\gamma^h}$ for all $p \in P_1(\mathbf{R}^d)$ and $G_{i,\gamma}(\boldsymbol{q}(\boldsymbol{x})) = \boldsymbol{q}(\boldsymbol{x})\big|_{\sigma_\gamma^h}$ for all $\boldsymbol{q} \in [P_0(\mathbf{R}^d)]^d$. A simple definition of $E_{i,\gamma}$, which satisfies this requirement is the linear extension

$$(E_{i,\gamma}u_i^h)(\boldsymbol{x}_\gamma) = \begin{cases} u_i^h(\boldsymbol{x}_\gamma^\perp) + \nabla u_i^h(\boldsymbol{x}_\gamma^\perp)\cdot(\boldsymbol{x}_\gamma - \boldsymbol{x}_\gamma^\perp) & \text{if } \boldsymbol{x}_\gamma \notin \Omega_i \\ u_i^h(\boldsymbol{x}_\gamma) & \text{if } \boldsymbol{x}_\gamma \in \Omega_i \end{cases} \quad (6)$$

where $\boldsymbol{x}_\gamma \in \sigma_\gamma$ is a given point and $\boldsymbol{x}_\gamma^\perp \in \sigma_i$ is the "closest" point on σ_i. Similarly, we define $G_{i,\gamma}$ to be an extension by a constant, i.e., given $\boldsymbol{x}_\gamma \in \sigma_\gamma$ we define

$$(G_{i,\gamma}\nabla u_i^h)(\boldsymbol{x}_\gamma) = \nabla u_i^h(\boldsymbol{x}_\gamma^\perp). \quad (7)$$

Finally, we note that although g_1 and g_2 belong in the same space $L^2(\sigma)$, their discretization requires two separate discrete control spaces $L^{2,h}_{1,\sigma}$ and $L^{2,h}_{2,\sigma}$, defined on σ_1 and σ_2, respectively. Here we choose $L^{2,h}_{i,\sigma}$ to be a piecewise constant space on σ_i^h, which is consistent with the piecewise linear discretization in Ω_i. These considerations yield the following extension of (3) to non-coincident interfaces:

$$\begin{aligned} J_\delta^h(u_1^h,u_2^h,g_1^h,g_2^h) &= \frac{\beta_1}{2}\int_{\sigma_1}(u_1^h - E_{2,1}u_2^h)^2 dS + \frac{\beta_2}{2}\int_{\sigma_2}(u_2^h - E_{1,2}u_1^h)^2 dS \\ &+ \frac{\gamma_1}{2}\int_{\sigma_1}((\kappa_1\nabla u_1^h - \kappa_2 G_{2,1}\nabla u_2^h)\cdot\mathbf{n}_1)^2 dS + \frac{\gamma_2}{2}\int_{\sigma_2}((\kappa_1 G_{1,2}\nabla u_1^h - \kappa_2\nabla u_2^h)\cdot\mathbf{n}_2)^2 dS \\ &+ \frac{\rho}{2}\left(\int_{\sigma_1} g_1^h dS + \int_{\sigma_2} g_2^h dS\right)^2 + \frac{\delta_1}{2}\int_{\sigma_1}(g_1^h)^2 dS + \frac{\delta_2}{2}\int_{\sigma_2}(g_2^h)^2 dS. \end{aligned} \quad (8)$$

The first two pairs of terms in (8) generalize the state misfit and the flux misfit terms in (3), and the fifth term controls the total flux misfit between the interfaces. The last two terms generalize the control penalties necessary for the well-posedness of the optimization problem. The discretization of (4) on non-coincident interfaces is thus given by the following problem:

$$\begin{gathered} \text{minimize} \quad J_\delta^h(u_1^h,u_2^h,g_1^h,g_2^h) \text{ over } H^h_{1,\Gamma}\times H^h_{2,\Gamma}\times L^{2,h}_{1,\sigma}\times L^{2,h}_{2,\sigma} \\ \text{subject to a discretized form of the weak equations (2).} \end{gathered} \quad (9)$$

Recovery of globally linear fields is desirable for any numerical method for (1). However, in order to pass this linear "patch test", methods based on Lagrange multipliers require carefully constructed multiplier spaces [7] and/or additional modifications of the interface grids [4, 8]. An attractive property of (9) is that it does not require any additional considerations to pass a patch test: recovery of globally linear fields is built into the virtual control formulation.

Theorem 1. *Assume that $\kappa_1 = \kappa_2$ and that the discrete interfaces have matching boundaries, i.e., $\partial\sigma_1 = \partial\sigma_2$. Then, in the limit $\delta_i \to 0$, (9) recovers exactly any globally linear solution u_ℓ of (1).*

Proof. We show that $u^h_{i,\ell} = u_\ell\big|_{\sigma_i}$ and $g^h_{i,\ell} = \mathbf{n}_i \cdot \nabla u^h_{i,\ell} = \mathbf{n}_i \cdot \nabla u_\ell\big|_{\sigma_i}$, $i = 1, 2$ is an optimal solution of (9). Since any conforming discretization of (2) recovers linear solutions, $u^h_{i,\ell}$ is feasible. By construction $E_{i,\gamma}$ and $G_{i,\gamma}$ are exact for linear and constant fields, respectively and so, the first four terms in (8) vanish, i.e.,

$$J^h_\delta(u^h_{1,\ell}, u^h_{2,\ell}, g^h_{1,\ell}, g^h_{2,\ell}) = \\ \frac{\rho}{2}\left(\int_{\sigma_1} g^h_{1,\ell} dS + \int_{\sigma_2} g^h_{2,\ell} dS\right)^2 + \frac{\delta_1}{2}\int_{\sigma_1} (g^h_{1,\ell})^2 dS + \frac{\delta_2}{2}\int_{\sigma_2} (g^h_{2,\ell})^2 dS.$$

Since u_ℓ is linear $\nabla u^h_{i,\ell} = \boldsymbol{c}$ for some $\boldsymbol{c} \in \mathbf{R}^d$, $d = 2, 3$. Let $\boldsymbol{u}^\perp_\ell \in \mathbf{R}^3$ be a linear vector field such that $\nabla \times \boldsymbol{u}^\perp_\ell = \boldsymbol{c}$. Stokes' theorem and $\partial\sigma_1 = \partial\sigma_2$ imply that

$$\int_{\sigma_1} \mathbf{n}_1 \cdot \nabla u^h_{2,\ell} dS = \int_{\sigma_1} \mathbf{n}_1 \cdot \nabla \times \boldsymbol{u}^\perp_\ell dS = \int_{\partial\sigma_1} \boldsymbol{u}^\perp_\ell \cdot dl \\ = -\int_{\partial\sigma_2} \boldsymbol{u}^\perp_\ell \cdot dl = -\int_{\sigma_2} \mathbf{n}_2 \cdot \nabla \times \boldsymbol{u}^\perp_\ell dS = -\int_{\sigma_2} \mathbf{n}_2 \cdot \nabla u^h_{2,\ell} dS,$$

In two-dimensions the same identity follows by choosing a linear function $u^\perp_\ell$ such that $\nabla u^\perp_\ell = \boldsymbol{c}^\perp = (-c_2, c_1)$. Thus, we have that

$$J^h_\delta(u^h_{1,\ell}, u^h_{2,\ell}, g^h_{1,\ell}, g^h_{2,\ell}) = \frac{\delta_1}{2}\int_{\sigma_1} (g^h_{1,\ell})^2 dS + \frac{\delta_2}{2}\int_{\sigma_2} (g^h_{2,\ell})^2 dS.$$

The theorem follows by taking the limit $\delta_i \to 0$.

3.1 Solution of the discrete optimization problem

Let $\boldsymbol{u}_i$, $\boldsymbol{g}_i$ denote the coefficient vectors of the states u^h_i and controls g^h_i, respectively. Setting $\vec{\boldsymbol{u}} = (\boldsymbol{u}_1, \boldsymbol{u}_2)$ and $\vec{g} = (\boldsymbol{g}_1, \boldsymbol{g}_2)$, the virtual control formulation (9) is equivalent to the Quadratic Programming problem (QP)

$$\underset{\vec{\boldsymbol{u}}, \vec{\boldsymbol{g}}}{\text{minimize}} \quad \mathbf{J}_\delta(\vec{\boldsymbol{u}}, \vec{\boldsymbol{g}}) \quad \text{subject to} \quad \begin{cases} K_1\boldsymbol{u}_1 = \boldsymbol{f}_1 - G_1\boldsymbol{g}_1 \\ K_2\boldsymbol{u}_2 = \boldsymbol{f}_2 + G_2\boldsymbol{g}_2 \end{cases}, \tag{10}$$

where K_i is the finite element stiffness matrix, $\boldsymbol{f}_i$ is the finite element load vector, $\boldsymbol{g}_i$ is the external load vector induced by the control g_i, and

$$\mathbf{J}_\delta(\vec{\boldsymbol{u}}, \vec{\boldsymbol{g}}) = \frac{1}{2}\vec{\boldsymbol{u}}^T H \vec{\boldsymbol{u}} + \vec{\boldsymbol{g}}^T M \vec{\boldsymbol{g}}$$

with suitable H and M. For clarity we have subsumed the weights β_i, γ_i and the penalty coefficients δ_i into the matrices H and M.

Because K_1 and K_2 are discretizations of mixed Dirichlet-Neumann boundary value problems they are invertible. Thus, we solve (10) by a reduced space approach, i.e., we eliminate the states by solving the constraint equations:

$$\boldsymbol{u}_i = K_i^{-1}\left(\boldsymbol{f}_i + \boldsymbol{g}_i\right), \quad i = 1, 2. \tag{11}$$

This yields an equivalent *unconstrained* optimization problem

$$\underset{\vec{\boldsymbol{g}}}{\text{minimize}} \qquad \frac{1}{2}\vec{\boldsymbol{g}}^T H_{\text{red}}\,\vec{\boldsymbol{g}} + \vec{\boldsymbol{g}}^T \boldsymbol{f}_{\text{red}}\,, \tag{12}$$

in terms of the virtual Neumann controls only. Setting the first variation of (12) to zero yields the following necessary condition

$$H_{\text{red}}\,\vec{\boldsymbol{g}} = \boldsymbol{f}_{\text{red}} \tag{13}$$

for the optimal virtual Neumann control. Since the dimensions of H_{red} and $\boldsymbol{f}_{\text{red}}$ equal the dimension of the virtual control vector $\vec{\boldsymbol{g}} = (\boldsymbol{g}_1, \boldsymbol{g}_2)$, the size of (13) is much smaller than the size of the optimality system of the original QP (10).

We solve (13) iteratively using GMRES, which requires the application of the reduced Hessian H_{red}. The latter involves multiple inversions of the stiffness matrices K_i. In our case, these matrices correspond to discretizations of second-order elliptic operators and so, they can be preconditioned by a number of algebraic and geometric multigrid preconditioners. Once the solution $\vec{\boldsymbol{g}} = (\boldsymbol{g}_1, \boldsymbol{g}_2)$ has been computed, one can recover the state variables from (11).

4 Numerical Results

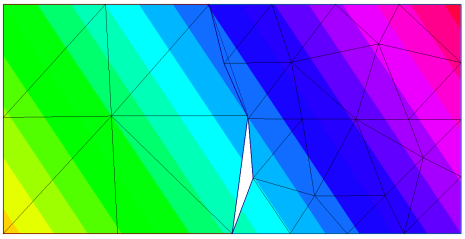

Fig. 2. Globally linear solution for an S-curve interface containing large gaps and overlaps.

We present three preliminary numerical studies of the virtual control formulation (9). These studies verify Theorem 1 and examine the convergence rates of the virtual control formulation for different interface configurations. In all cases we discretize the subdomain equations (2) using independently defined partitions Ω_i^h of Ω_i into affine triangles and standard C^0 piecewise linear nodal elements. Then we solve the QP (10) using the equivalent reduced-space formulation (12). This involves solving the optimality system (13) for the two Neumann controls by GMRES and then recovering the optimal states. We solve the reduced Hessian system to a relative residual of $1e$-15. The optimization-based method is implemented in FreeFem++ [9].

Linear patch test. The first study confirms numerically Theorem 1, i.e., the ability of (9) to recover globally linear solutions. To this end, we set $u = 3x + 2y$

and define the Dirichlet boundary condition data and the right hand side by inserting this solution in (1). Then we set $\delta_1 = \delta_2 = 0$ and solve (9) for several different interface configurations. In general the well-posedness of (9) may require positive penalty parameters. However, in the case of the linear patch test, the optimization problem remained well-posed with $\delta_1 = \delta_2 = 0$. We note that in some related contexts, such as optimization-based additive operator splitting [10], one can prove that the associated optimization formulation is well-posed without control penalties. In all cases (9) recovers the exact solution to machine precision. Figure 2 shows this solution when the induced interface grids have a $2:3$ ratio of elements. Despite the obvious gaps and overlaps between the interface grids we see a perfect recovery of the linear function.

Convergence study. To study the convergence of (9) we use the method of manufactured solutions on a domain with an S-curve interface; see Figure 3. We set the exact solution of (1) to be the following function:

$$u = x^2(y-2)^3\sin(2\pi x) - (x-3)^3\cos(2\pi x - y). \tag{14}$$

Substitution of (14) into the interface problem (1) defines the right hand sides and Dirichlet boundary conditions for the subdomain problems. We measure the errors of the optimal finite element state variables u_i^h against the exact solution u_{ex} of (1) using sums of L^2 and H^1 norms on the discretized subdomains, i.e., we consider the following compound error norms:

$$\left\|u_i^h - u_{ex}\right\|_0^2 := \sum_{i=1}^{2} \left\|u_i^h - u_{ex}\right\|_{0,\Omega_i^h}^2; \quad \left\|u_i^h - u_{ex}\right\|_1^2 := \sum_{i=1}^{2} \left\|u_i^h - u_{ex}\right\|_{1,\Omega_i^h}^2. \tag{15}$$

This study investigates the accuracy of the method when subdomain meshes have different resolutions. We consider several combinations of Ω_i^h providing a representative range of ratios $|\sigma_1^h| : |\sigma_2^h|$ between the numbers of elements in the discrete interfaces σ_1^h and σ_2^h. We compute the optimal finite element states on a sequence of six successively refined grids on Ω_1 and Ω_2. While the grids are defined independently on each subdomain by using the FreeFem++ mesh generator, the ratio of their interface segments $|\sigma_1^h| : |\sigma_2^h|$ is kept constant. This is accomplished by starting with an initial vertex distribution along $\partial\Omega_1$ and $\partial\Omega_2$, which produces the desired ratio $|\sigma_1^h| : |\sigma_2^h|$, and then driving the mesh refinement through doubling the number of vertices on the subdomain boundaries. We consider a total of eight different ratios in this study. For all interface ratios in this study we set $\beta_1 = \beta_2 = \gamma_1 = \gamma_2 = \rho = 1$, and $\delta_1 = \delta_2 = 1e\text{-}10$ in the objective (8).

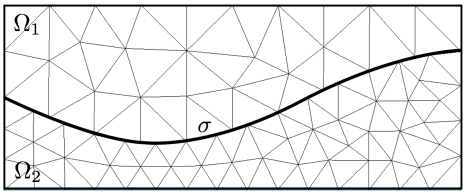

Fig. 3. An S-curve interface containing small gaps and overlaps. This is an example of grids having a 2:3 ratio of elements on the interface.

Results in Figure 4 reveal first order convergence in both compound norms. We believe that the suboptimal L^2 rate is due to the choice of piecewise constant

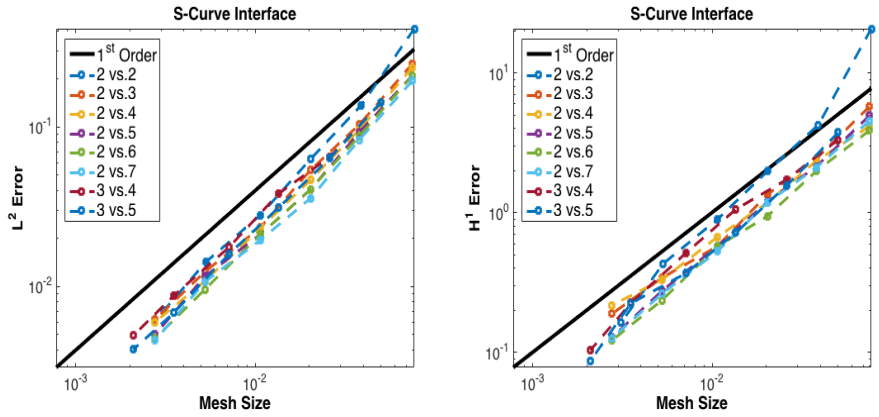

Fig. 4. Convergence rates of (9) for interface grids having different element ratios. In each case the interface element ratio $|\sigma_1^h| : |\sigma_2^h|$ is preserved throughout the grid refinement process.

controls g_i^h. Although this choice is enough to pass a linear patch test (see Theorem 1), it limits the accuracy of the finite element solution in the subdomain equations. In future work we will investigate a variant of the algorithm, which uses more accurate control representations.

Flux conservation. Our last example examines global flux conservation across the interface as a function of the parameter ρ in the objective functional (8). We set $\delta_1 = \delta_2 = 1e\text{-}10$ in (8) and use the S-curve interface in Fig. 3 with a sequence of refined grid from the convergence study with $|\sigma_1^h| : |\sigma_2^h|$ ratio of 2:3. Results in Table 1 compare the compound norm errors and global flux conservation, as measured by the global flux mismatch

$$\Delta g = \left(\int_{\sigma_1} g_1 \, dS - \int_{\sigma_2} g_2 \, dS \right)^2 ,$$

for a small ($\rho = 1e-3$), medium ($\rho = 1$) and large ($\rho = 1e+3$) values of the parameter ρ. We observe significant improvements in the global flux conservation over *non-coincident* interfaces as the value of this parameter increases. At the same time, the compound norm errors remain the same for all three cases, i.e., the accuracy of the solution is not affected by increasing the weight of the flux mismatch in the objective.

Parameter	**ρ=1e-3**			**ρ=1**			**ρ=1e+3**		
h	L^2	H^1	Δg	L^2	H^1	Δg	L^2	H^1	Δg
7.512e-2	2.495e-1	5.727e-0	3.264e-9	2.495e-1	5.727e-0	3.264e-15	2.495e-1	5.727e-0	3.267e-21
3.801e-2	1.036e-1	2.435e-0	1.408e-7	1.036e-1	2.435e-0	1.408e-13	1.036e-1	2.435e-0	1.408e-19
2.023e-2	5.337e-2	1.301e-0	4.072e-1	5.370e-2	1.349e-0	5.513e-7	5.370e-2	1.349e-0	5.515e-13
1.070e-2	2.356e-2	5.711e-1	1.118e-2	2.353e-2	5.751e-1	1.233e-8	2.353e-2	5.751e-1	1.234e-14
5.251e-3	1.240e-2	3.422e-1	3.154e-7	1.240e-2	3.422e-1	3.159e-13	1.240e-2	3.422e-1	3.159e-19
2.770e-3	6.236e-3	1.896e-1	2.772e-6	6.236e-3	1.896e-1	2.788e-12	6.236e-3	1.896e-1	2.788e-18

Table 1. Solution error and global flux conservation as functions of ρ.

5 Conclusions

We have developed a new, virtual control formulation for discrete transmission and mesh tying problems with non-coincident discrete interfaces. The method is linearly consistent, while a moderate weight in the objective ensures conservation of the global flux between the subdomains to machine precision and *without any additional interface manipulations*. Preliminary results reveal first-order accuracy in compound L^2 and H^1 norms. Future work will consider more accurate choices for the virtual controls to improve the L^2 convergence rates.

Acknowledgments

This material is based upon work supported by the U.S. Department of Energy, Office of Science, Office of Advanced Scientific Computing Research, and the Laboratory Directed Research and Development program at Sandia National Laboratories.

References

1. Farhat, C., Lesoinne, M., Tallec, P.L.: Load and motion transfer algorithms for fluid/structure interaction problems with non-matching discrete interfaces: Momentum and energy conservation, optimal discretization and application to aeroelasticity. Comput. Methods Appl. Mech. Engrg. **157**(1–2) (1998) 95 – 114
2. de Boer, A., van Zuijlen, A., Bijl, H.: Review of coupling methods for non-matching meshes. Comput. Methods Appl. Mech. Engrg. **196**(8) (2007) 1515 – 1525
3. Dohrmann, C.R., Key, S.W., Heinstein, M.W.: A method for connecting dissimilar finite element meshes in two dimensions. Int. J. Numer. Meth. Eng. **48**(5) (2000) 655–678
4. Dohrmann, C.R., Key, S.W., Heinstein, M.W.: Methods for connecting dissimilar three-dimensional finite element meshes. Int. J. Numer. Meth. Eng. **47**(5) (2000) 1057–1080
5. Gunzburger, M.D., Peterson, J.S., Kwon, H.: An optimization based domain decomposition method for partial differential equations. Computers & Mathematics with Applications **37**(10) (1999) 77 – 93
6. Gunzburger, M.D., Lee, H.K.: An optimization-based domain decomposition method for the Navier-Stokes equations. SIAM Journal on Numerical Analysis **37**(5) (2000) pp. 1455–1480
7. Laursen, T.A., Heinstein, M.W.: Consistent mesh tying methods for topologically distinct discretized surfaces in non-linear solid mechanics. Int. J. Numer. Meth. Eng. **57**(9) (2003) 1197–1242
8. Parks, M., Romero, L., Bochev, P.: A novel lagrange-multiplier based method for consistent mesh tying. Comput. Methods Appl. Mech. Engrg. **196**(35–36) (2007) 3335 – 3347
9. Hecht, F.: New development in freefem++. J. Numer. Math. **20**(3-4) (2012) 251–265
10. Bochev, P., Ridzal, D.: Optimization-based additive decomposition of weakly coercive problems with applications. Computers & Mathematics with Applications **71**(11) (2016) 2140 – 2154